Kinetic modeling of the simultaneous etherification of ethanol with C_4 and C_5 olefins over Amberlyst™ 35 using model averaging

Rodrigo Soto[a], Carles Fité[a,]*, Eliana Ramírez[a], Roger Bringué[a], Fidel Cunill[a]

[a]*Chemical Engineering Department. Faculty of Chemistry. University of Barcelona. Martí i Franquès 1-11, 08028-Barcelona.* *Corresponding author: Tel.: +34934034769, Fax: +34934021291

Email addresses: r.soto@ub.edu (R. Soto), fite@ub.edu (C. Fité), eliana.ramirez-rangel@ub.edu (E. Ramírez), rogerbringue@ub.edu (R. Bringué), fcunill@ub.edu (F. Cunill).

Graphical abstract

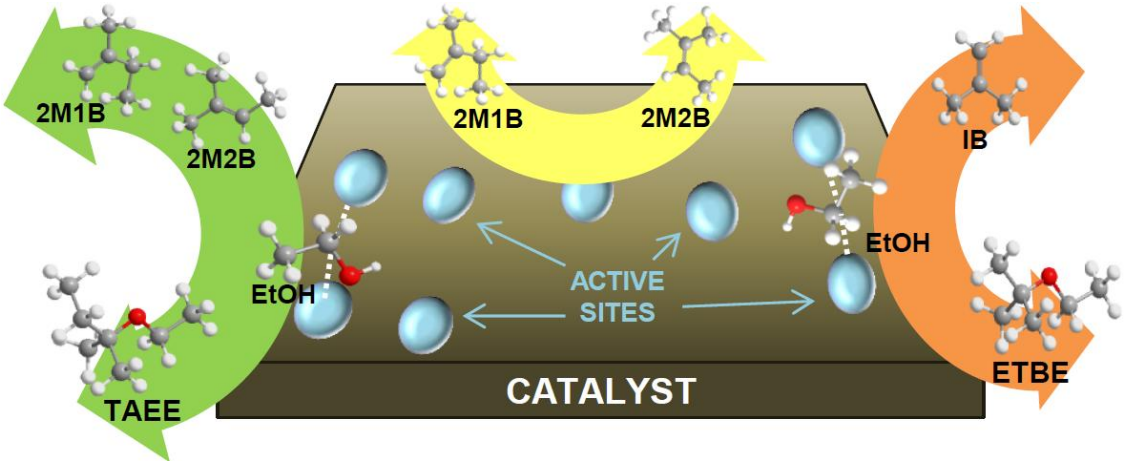

Highlights

- Model averaging provides the kinetic model taking into account model uncertainty
- ETBE is formed faster than TAEE in the simultaneous etherification
- Reactions mechanism is deduced from the proposed kinetic model
- Active sites are mainly occupied by adsorbed ethanol, ETBE and TAEE
- Two active sites participate in etherification reactions, and one in isomerization

Abstract

A kinetic study on the simultaneous liquid-phase etherification of ethanol with isobutene (IB), 2-methyl-1-butene (2M1B) and 2-methyl-2-butene (2M2B) catalyzed by Amberlyst™ 35 to form ethyl *tert*-butyl ether (ETBE) and *tert*-amyl ethyl ether (TAEE) is presented. Isothermal experimental runs were carried out in a stirred tank batch reactor in the temperature range 323-353 K at 2.0 MPa, starting from different initial concentrations. Obtained reaction rates were free of catalyst load, internal, and external mass transfer effects. Mathematical fitting of a series

of systematically originated models, model selection, and model averaging procedures were applied to find the best model and to draw conclusions about the reaction mechanism. The selected model involves a saturated catalytic surface with the participation of two active sites in etherification reactions and one active site in isoamylenes isomerization. Apparent activation energies for ETBE formation from IB and EtOH, TAEE formation from 2M1B and EtOH, TAEE formation from 2M2B and EtOH, and double bond isomerization between 2M1B and 2M2B were 72.8±1.4, 74.9±2.8, 81.2±2.2 and, 76.5±7.2 kJ/mol, respectively. The alkenes with the double bond in terminal position were more reactive towards EtOH than 2M2B, with the double bond in internal position.

Keywords: Kinetic modeling; Model averaging; Ethyl *tert*-butyl ether; *tert*-Amyl ethyl ether; Simultaneous etherification; Amberlyst™ 35.

1. Introduction

Tertiary alkyl ethers production using ion-exchange resins is an important example of industrial heterogeneous catalysis, because it is widely applied process due to the environmental interest in such compounds as high performance additives for fuels. New interesting processes of simultaneous production of several ethers in the same reaction unit are feasible [1–6], and they could become an industrial reality in the forthcoming years. Promising conclusions have been drawn regarding thermodynamics and product distribution at experimental conditions of industrial interest. Kinetic studies on such complex etherification systems allow to determine the mechanisms taking place on catalytic surfaces.

Several studies have been focused hitherto on the kinetics of isolated liquid-phase formation of ethanol-based tertiary ethers over acidic ion-exchange resins. For instance, Fité et al. [7] presented an Eley-Rideal (ER) mechanism for the synthesis of ethyl *tert*-butyl ether (ETBE) from isobutene (IB) and ethanol (EtOH). Françoisse and Thyrion [8] found a change in the kinetic mechanism depending on the EtOH concentration for ETBE synthesis. Linnekoski and Krause [9] proposed a Langmuir-Hinshelwood-Hougen-Watson (LHHW) mechanism for the synthesis of *tert*-amyl ethyl ether (TAEE) from isoamylenes (IA) and EtOH. Further progress was made by Oktar et al. [10] and Zhang et al. [1] concerning TAEE formation reactions. The influence of the reaction medium on etherification reactions was also studied [7,11–14], and adsorption equilibrium and also kinetic parameters were estimated [15]. More recently, reviews on ETBE [16] and TAEE [17] isolated syntheses gathered the main progresses and the future prospects for the synthesis of these ethers.

Apart from using bioethanol and reducing the harmful C_5 isolefins content in fuel, the simultaneous production of ETBE and TAEE as one-pot synthesis brings about the versatility to adapt production targets depending on either the desired final fuel volatility or the refinery needs [18]. The involved reaction mechanisms, kinetics and thermodynamics determine the product distribution and, therefore, they are key factors for setting industrial operating conditions and understanding the catalytic behavior. However, to the best of our knowledge, there is a lack of information about detailed kinetic studies regarding the simultaneous production of several ethers, and more specifically focused on the simultaneous production of ETBE and TAEE. In the search of the kinetic equations that describe experimental data, and due to the simultaneous occurrence of the involved chemical reactions, a considerably large number of combinations of kinetic expressions can be proposed. To make sure that a good kinetic model candidate is not neglected, a systematic kinetic analysis should be the first step for fitting the experimental data. Then, model selection and model averaging can be applied to obtain a reliable kinetic model from a set of candidate models [19–24].

Based on the mentioned reasons, the aim of this work is to study the kinetics of the simultaneous liquid-phase synthesis of ETBE and TAEE from a pure isoolefins feedstock and EtOH over Amberlyst™ 35. The main goals are to find the best kinetic model, to estimate the kinetic parameters, to extract mechanistic conclusions based on LHHW or ER formalisms, and to compare it with the isolated production of both ethers.

2. Experimental section

2.1. Experimental setup

The experimental setup consisted of a 200 mL stirred tank batch reactor equipped with a six-blade magnetic stirrer (Autoclave Engineers; Erie, PA, USA). The working temperature range was 323-353K, controlled within ±0.1K by means of a thermostatic bath mixture (33 vol.% of 1,2-propanediol and rest of water). The reactor pressure was maintained at 2.0 MPa with nitrogen to widely exceed the vapor pressure of the reaction mixture at the highest assayed temperature, and to allow impelling samples of the reaction medium from the reactor to the gas chromatograph through the piping system. A detailed scheme and further information about the setup can be found in the Supplementary Material section.

2.2. Reactants

The following reagents were used in all the runs: a mixture of IA, composed by 2-methyl-2-butene (2M2B, 96% G.C.) and 2-methyl-1-butene (2M1B, 4% G.C.; TCI Europe, Belgium), IB

(>99.9% G.C.; Air Liquide, Spain) and absolute dry EtOH (max. 0.02 wt.% of water; Panreac, Spain).

Chemical standards used for analytical procedures were: 2,4,4-trimethyl-1-pentene (TMP-1, >98.0% G.C.; Fluka, Buchs, Switzerland), 2,4,4-trimethyl-2-pentene (TMP-2, >98%G.C.; Fluka, Buchs, Switzerland), *tert*-amyl alcohol (TAA, >98.0% G.C.; TCI Europe, Belgium), *tert*-butyl alcohol (TBA, >99.7% G.C.; TCI Europe, Belgium), ETBE (>99.0% G.C.; TCI Europe, Belgium), 2M1B (>99.0% G.C.; TCI Europe, Belgium), and 2M2B (>99% G.C.; Sigma Aldrich, Germany). TAEE (99.5% G.C.) and C_5 dimers (>99.5% G.C.) were obtained and purified in our lab after successive distillations in a packed column.

2.3. Catalyst

Amberlyst™ 35 (A-35; Rohm & Haas, Chauny, France) was used as the acidic macroreticular resin catalyst, since it is a very active catalyst in etherification reactions [25] with high acid capacity (5.32 eq $H^+ \cdot kg^{-1}$). The main physical and structural properties of the commercial catalyst are described elsewhere [4]. Prior to the experimental runs, the catalyst was dried 2.5 h in an atmospheric oven at 383 K and subsequently 15 h in a vacuum oven at 383 K. The remaining water content in the catalyst after pretreatment was measured by Karl Fischer titration method for different samples of A-35 with an average result of less than 3.5%-wt.

2.4 Analytical Method

Samples were taken in-line from the reaction medium through a sampling valve (Valco A2CI4WE.2; VIVI AG International, Schenkon, Switzerland), which injected 0.2 μL of pressurized liquid into a gas-liquid chromatograph (Agilent 6890 GC; Madrid, Spain) equipped with a capillary column (HP-PONA 19091S-001, 100% dimethylpolysiloxane, 50.0 m x 0.2 mm x 0.5 μm nominal; Hewlett Packard, Palo Alto, CA, USA). A mass selective detector (HP 5973N MS; Hewlett Packard, Palo Alto, CA, USA) coupled to the GC was used to identify and quantify the reaction system components. When detected, $C_{4\text{-}5}$ codimers and C_5 dimers were lumped together, each as a group of compounds.

2.5 Experimental procedure

The initial molar ratios of alcohol to olefins ($R^o_{A/O}$) and of IB to IA ($R^o_{C4/C5}$) were both varied from 0.5 to 2. The working temperature ranged from 323 to 353 K. The reactor was isothermal during each experimental run. A dry catalyst mass of 0.25, 0.4, 1 and 1.5 g of A-35 was used for kinetic experiments at 353, 343, 333 and 323 K, respectively. These catalyst loads allowed to obtain kinetic data with enough accuracy during the runs duration. All the preliminary

experiments to evaluate the possible effect of mass transfer and catalyst load were conducted at the highest assayed temperature (353 K), where these effects are more noticeable.

In each run, the initial reaction mixture of EtOH and olefins was placed into the reactor, pressurized to 1.0 MPa with N_2, and heated up to the desired reaction temperature. It was verified that no reaction takes place in the absence of catalyst. The weighted mass of previously pretreated catalyst was placed in the catalyst injector, pressurized with N_2 to 2.0 MPa and injected into the reactor by means of pressure difference. Immediately after, the reactor pressure was set to 2.0 MPa. That instant was considered the starting (zero) time. At different reaction times, samples were taken in-line by pressure difference and analyzed by GC/MS.

2.6 Calculations and experimental uncertainty

Reactants conversion (X_j) was calculated at a given time by means of Eq. 1:

$$X_j = \frac{\text{reacted mole of } j}{\text{initial mole of } j} \tag{1}$$

Experimental reaction rates were estimated from the mole evolution profile for each compound by means of Eq. 2, where r_j is the formation rate of compound j, W_{cat} is the dry catalyst mass, and n_j is the mole number of compound j:

$$r_j = \frac{1}{W_{cat}} \frac{dn_j}{dt}\bigg|_t \tag{2}$$

The run at $R^o_{A/O}$=1, $R^o_{C4/C5}$=1 and 343 K was replicated three times and an experimental uncertainty of 6% in mole basis was estimated for a 95% confidence level. Maximum experimental uncertainties of 6% and 12% were estimated for r_{ETBE} and r_{TAEE}, respectively, for the same confidence level. It can be assumed that the experimental error of non-replicated experiments would be of the same order. The mass balance was always fulfilled within ± 4%. As these values of experimental error are acceptable, experiments were considered reproducible and reliable.

3. Results and Discussion

3.1 Reaction system

Besides the simultaneous etherification of IB and IA with EtOH and IA isomerization, some side reactions, namely olefins hydration and oligomerization, could take place depending on the temperature and the initial reactants concentration [6]. The experimental conditions in the

present work were chosen to avoid these side reactions, as confirmed by the extremely low presence of byproducts in the chemical analyses. For this reason, only the system of parallel reactions depicted in Fig. 1 was considered for kinetic modeling. R1 is the etherification of IB with EtOH to form ETBE, R2 and R3 are, respectively, the etherifications of 2M1B and 2M2B with EtOH to form TAEE, and R4 is the double bond isomerization reaction between 2M1B and 2M2B. According to Fig. 1, the global reaction rate of TAEE formation is expressed as $r_{TAEE}=r_{R2}+r_{R3}$, and the formation rate of 2M2B is expressed as $r_{2M2B}=r_{R4}-r_{R3}$.

Figure 1

3.2 Effect of internal and external mass resistances

In order to find out the experimental conditions for which the effects of internal and external mass transfers (IMT and EMT) can be neglected, a set of preliminary experiments was carried out at $R^o_{A/O}=1$, $R^o_{C4/C5}=1$, 353K, and using 1 g of pretreated A-35. The effect of IMT was evaluated for different ranges of particle size, obtained by crashing and sieving the catalyst. The effect of EMT was tested by varying the stirring speed from 600 to 800 rpm, based on previous studies on isolated ETBE and TAEE syntheses [9,26,27]. Fig. 2 plots the initial etherification rates, where IMT and EMT effects are expected to be more noticeable, calculated for ETBE and TAEE as a function of the inverse of the average catalyst particle diameter ($1/d_p$) at different stirring speeds.

Figure 2

Results in Fig. 2 indicate that mass transfer effects are negligible for particle size below 0.4 mm and stirring speed above 600 rpm. Consequently, a catalyst bead size of 0.25-0.4 mm and a stirring speed of 600 rpm have been used in the next stages of this study.

3.3 Effect of the catalyst load

The effect of the catalyst load (CL) was also evaluated in preliminary experiments at $R^o_{A/O}=1$, $R^o_{C4/C5}=1$, 353K, 600 rpm, and using catalyst particle sizes of 0.25-0.4 mm. Assayed catalyst loads were 0.25, 1 and 2 g of dried A-35. Fig. 3 depicts the obtained reactants conversion for the different catalyst loads as a function of the standardized time, named as contact time, and used for comparative purposes. Since the obtained curves for different catalyst loads overlap, it can be concluded that the effect of CL up to 2 g of catalyst is negligible under the explored experimental conditions. Consequently, catalyst loads used for subsequent kinetic experiments were below 2 g, specifically 0.25, 0.4, 1, and 1.5 g at 353, 343, 333, and 323 K, respectively.

Figure 3

3.4 Mole evolution in the kinetic experiments

A total set of 21 experiments (including replications) were carried out free of IMT, EMT and CL effects. Examples of the mole evolution profiles obtained under several experimental conditions are depicted in Fig. 4. In all runs, the amount of formed ETBE mole exceeded TAEE mole.

Figure 4

Since water is known to inhibit etherification reactions and to promote tertiary alcohols (TBA and TAA) formation [4], special care was taken to minimize water sources: absolute dry EtOH was used as reactant, and the catalyst was dried under vacuum before its use. The amount of formed tertiary alcohols detected as the result of the remaining water content of the catalyst after pretreatment and the small water content in EtOH, was very low, the molar fractions of TBA and TAA being always lower than 0.003 and 0.001, respectively. Olefins dimers were formed only in the experiments at the highest explored temperature and initial stoichiometric excess of olefins, though in very low extent (molar fraction lower than 0.002). Therefore, it can be assumed that kinetic data for etherification reactions, obtained in a wide range of compositions and temperatures, were not affected by side reactions.

3.5 Kinetic results

3.5.1 Experimental reaction rates

Initial reaction rates of reactants and products, estimated from Eq. 2, are gathered in Table 1. Initial etherification rates data obtained are in concordance with the experimental values determined for the isolated syntheses of ETBE and TAEE over similar catalysts [7,28,29]. As it can be seen, the lower the temperature, the lower the etherification rates obtained, as expected from the Arrhenius relationship. ETBE production took place readily compared to global formation of TAEE. At $R^o_{A/O}$=1 and $R^o_{C4/C5}$=1, the rate ratio r^0_{ETBE}/r^0_{TAEE} (Table 1) slightly decreased at increasing temperature, what indicates a higher activation energy for TAEE formation compared to ETBE formation. Estimated r^0_{TAEE} was generally faster than $-r^0_{2M2B}$. As for EtOH initial consumption rate, it is confirmed that it corresponds to the sum of initial formation rates of ETBE and TAEE ($-r^0_{EtOH} = r^0_{ETBE} + r^0_{TAEE}$) within the experimental error.

Table 1

Concerning the effect of EtOH concentration on etherification rates, it has been previously reported [7,30] that alcohols present a moderator or even inhibitory effect at high concentrations on the syntheses of tertiary ethers. It can be attributed to a disruption of the catalyst sulfonic groups network caused by the adsorbed alcohol molecules, which results in a slower mechanism than a concerted mechanism by totally undissociated sulfonic groups. TAEE formation was slightly more affected by $R^{o}_{A/O}$ than ETBE. At constant $R^{o}_{C4/C5}$=1 and 343 K, the ratio $r^{0}_{ETBE}/r^{0}_{TAEE}$ scarcely varied from 3.9 to 4.1 on increasing $R^{o}_{A/O}$ from 0.5 to 2 (Table 1). Focusing on the effect of olefins concentration on etherification rates at constant $R^{o}_{A/O}$, the higher the $R^{o}_{C4/C5}$, the higher the estimated r^{0}_{ETBE}. Accordingly, the analogous effect was observed between the initial IA concentration and r^{0}_{TAEE}. Concerning the rate ratio $r^{0}_{ETBE}/r^{0}_{TAEE}$ at 343 K and $R^{o}_{A/O}$=1, it decreased from 8.8 to 2.1 on decreasing $R^{o}_{C4/C5}$ from 2 to 0.5. These facts enforce the statement that olefins concentration presents a global positive kinetic order in etherification, whereas alcohol concentration presents a negative or close to zero kinetic order, in agreement with literature [29,30]. Fig. 5 plots the evolution with time of the experimental etherification rates obtained for several reaction temperatures when $R^{o}_{A/O}$ and $R^{o}_{C4/C5}$ are both equal to unity.

Figure 5

3.5.2 Kinetic modeling

3.5.2.1 Kinetic equations

A systematic methodology for evaluating the fitting of the kinetic equations based on the LHHW and RE formalisms was applied to the present study. All kinetic expressions evaluated for each reaction *i* were constructed according to the general form described by Eq.3. The kinetic term comprises the kinetic constant of reaction *i*, and it can include some adsorption equilibrium constant depending on the reaction mechanism; the driving force accounts for the distance to the chemical equilibrium; the adsorption term refers to the relative occupancy of the active sites by the adsorbed compounds; the resin-medium affinity term accounts for the interaction of the catalyst with the reaction medium; and *n* refers to the number of active sites or clusters of active sites that participate in the rate-controlling step of the proposed mechanism.

$$r_i = \frac{\{\text{Kinetic term}\}_i \cdot \{\text{Driving force}\}_i \cdot \{\text{Resin-medium affinity}\}}{\{\text{Adsorption term}\}^{n_i}} \qquad (3)$$

In the LHHW and RE formalisms, the kinetic term corresponds to the product of the intrinsic kinetic constant, the total concentration of active sites and, depending on the mechanism, some

adsorption equilibrium constants of the adsorbed species. All constants can be grouped in an apparent rate coefficient, k_i, for each reaction i.

The driving force of reaction i, is defined by Eq. 4, where a_j is the activity of compound j, ν_{ij} is the stoichiometric coefficient of the species j in reaction i, and K_i is the equilibrium constant of reaction i. Values of K_i have been taken from a previous study [5].

$$\left\{\text{Driving force}\right\}_i = \left(\prod_{j=1}^{\text{reactants}} a_j^{\nu_{ij}} - \frac{\prod_{j=1}^{\text{products}} a_j^{\nu_{ij}}}{K_i} \right) \tag{4}$$

The adsorption of reactants and desorption of products was supposed to be fast compared to surface reaction. Hence, the surface reaction was assumed as the rate-determining step. The use of activities instead of concentrations for non-ideal reaction mixtures in mechanistic expressions has been widely accepted. Activities of involved compounds in the reaction medium were estimated by means of the UNIFAC-Dortmund predictive method [31–33].

The adsorption term accounts for the relative occupancy of the catalyst active centers by the different adsorbed species and, therefore, it should be the same irrespectively of the considered reaction i. This term is expressed by Eq. 5, where K_j is the liquid-phase adsorption equilibrium constant of compound j, a_j is the activity of compound j, and S is the number of adsorbed species. Since compound activities are those of the liquid bulk phase, adsorption equilibrium constants in the kinetic equations describe the global effect of both the actual surface adsorption equilibrium constant, and the possible partition or distribution of involved species between the bulk phase and within the catalyst pores. The parameter α takes the value of 1 or 0, depending on whether the fraction of unoccupied active sites is considered as significant or not, respectively. The exponent of the adsorption term n_i has been considered to be equal to 1, 2, or 3, since these are the more plausible values [34,35].

$$\left\{\text{Adsorption term}\right\} = \alpha + \sum_{j=1}^{S} K_j \cdot a_j \tag{5}$$

An additional factor that can affect kinetics is the affinity between the reaction medium and the resin. A-35 consists of a flexible polymeric matrix where sulfonic groups are anchored. Since it is a non-rigid structure, its conformation can change depending on the physico-chemical nature of the reaction medium, leading to different swelling degree along the reaction time, because the reaction medium composition progressively changes. A more open resin backbone can enhance accessibility to inner active sites, and therefore the global catalytic activity of resin beads. This effect should be included in the kinetic equation, splitted from the kinetic constant, which

should not be composition dependent. The resin–medium affinity factor ψ, defined by the following expression, can account for this effect:

$$\{\text{Resin-medium affinity}\} = \psi = \exp\left(\frac{\overline{V_m}\ \phi_p^2}{RT}\left(\delta_m - \delta_p\right)^2\right) \quad (6)$$

The inclusion of ψ in the kinetic equation has been proved to enhance the prediction of the reaction rate equation for similar systems [14,28]. In Eq. 6, $\overline{V_m}$ is the mixture molar volume, estimated by the Hankinson-Brobst-Thomson (HBT) method [36]. ϕ_p is the catalyst porosity in the reaction medium, whose value has been taken as 0.5132 for A-35, determined by Inverse Exclusion Steric Chromatography (ISEC) in water [37]. δ_m and δ_p are the Hildebrand solubility parameter of the liquid mixture and the catalyst, respectively. The value of δ_m depends on the reaction medium composition and temperature, and it can be calculated by means of the following expression [38] :

$$\delta_m = \sum_j \Phi_j \cdot \delta_j = \sum_j \Phi_j \sqrt{\frac{\Delta_v H^\circ_j - RT}{\overline{V_j}}} \quad (7)$$

where Φ_j is the volume fraction of every compound *j* present in the reaction medium, with solubility parameter δ_j, $\Delta_v H^o_j$ is its molar enthalpy of vaporization, estimated at the run temperature by the methodology described in Yaws et al. [39], and $\overline{V_j}$ is its liquid molar volume in the medium, estimated by the HBT method.

It is to be noted that, in the search of the best kinetic equations, to include the possible case where the resin-medium interaction effect on kinetics is not significant, combinations with the term ψ equal to unity were also considered.

3.5.2.2 Temperature dependence of the parameters

The experimental runs have been carried out at different temperatures. Therefore, the parameters appearing in the kinetic equations have been expressed as a function of the temperature.

The adsorption equilibrium constant of species *j*, K_j, is expected to follow the Van't Hoff equation. Accordingly, the relation indicated in Eq. 8 has been considered. Parameters $K_{1,j}$ and $K_{T,j}$ are directly related to the adsorption entropy, $\Delta_{ads}S^\circ_j$, and enthalpy, $\Delta_{ads}H^\circ_j$, of compound *j* onto the active sites of the catalyst. These thermodynamic properties have been considered as constant, because of the relatively narrow studied temperature range, and the large number of

the fitted parameters in the kinetic equations, whose crosscorrelation would mask a possible temperature effect. The inverse of the mean temperature, $\overline{T}$, has been included to reduce the correlation between $K_{1,j}$ and $K_{T,j}$ in the fitting procedure, its value being 338.4 K.

$$K_j = \exp\left(\frac{\Delta_{ads}S^\circ{}_j}{R} - \frac{\Delta_{ads}H^\circ{}_j}{R}\left(\frac{1}{T}-\frac{1}{\overline{T}}\right)\right) = \exp\left(K_{1,j} + K_{T,j}\left(\frac{1}{T}-\frac{1}{\overline{T}}\right)\right) \quad (8)$$

As for the kinetic term, k_i, by considering that the intrinsic kinetic constant follows the Arrhenius law and the temperature dependence of the equilibrium adsorption constants (Eq. 8), it can be expressed by Eq. 9. Again, the inverse of the mean temperature, $\overline{T}$, was included to reduce the correlation between $k_{1,i}$ and $k_{T,i}$.

$$k_i = \exp\left(k_{1,i} + k_{T,i}\left(\frac{1}{T}-\frac{1}{\overline{T}}\right)\right) \quad (9)$$

In the resin-medium affinity term, the unknown parameter is the resin solubility parameter, δ_p. It has been reported that it follows a linear dependence with temperature in the assayed temperature range [14], and similarly to the solubility parameter dependency of pure species. Therefore, the following linear relation has been considered:

$$\delta_p = k_{D1} + k_{DT}\left(T - \overline{T}\right) \quad (10)$$

3.5.2.3 Proposed kinetic models

A kinetic model consists of a set of rate equations, being one per each reaction taking place, and consistent with the form indicated previously. Since reactions occur simultaneously on the same catalyst, the rate equations of a kinetic model have to present some common characteristics. The following assumptions have been applied for the different rate equations of a kinetic model:

i) For each reaction *i*, both parameters of the apparent kinetic constant, $k_{1,i}$ and $k_{T,i}$ (Eq. 9), have to be fitted, because the evolution of the reaction medium composition is highly temperature sensitive.

ii) The adsorption term is the same for all reactions, because it depends only on the reaction medium composition and temperature. The fraction of unoccupied sites could be significant (α=1) or not (α=0). The contribution of the adsorption of a given species *j* could be significant ($K_j \neq 0$) or non–significant (K_j=0); if significant, $K_{1,j} \neq 0$, and its temperature dependence could be relevant ($K_{T,j} \neq 0$) or not ($K_{T,j}$=0).

iii) The resin-medium affinity factor is the same for the kinetic equation of every reaction, because it would affect equally to catalyst activity. It could be significant ($\psi \neq 1$) or non-significant ($\psi=1$); if significant ($k_{D1}\neq 0$), the resin solubility parameter could be temperature sensitive ($k_{DT}\neq 0$) or non-sensitive ($k_{DT}=0$).

iv) Since the etherification reactions R1, R2, and R3 differ only on the olefin added to EtOH, the most plausible situation is that they proceed through the same mechanism, that is, the number of active sites participating in the rate-determining step, n_i, is the same. The isomerization reaction (R4) could involve a different number of active sites.

Consequently, the proposed kinetic models consist of all different combinations of equations 3 to 10 that fulfill the previous assumptions.

3.5.2.4 Multi-objective nonlinear least squares minimization

The estimation of the parameter values can be carried out by minimization of the sum of residual squares between experimental (r_i^{exp}) and calculated (r_i^{calc}) reaction rates for each reaction *i* (SRS_i). The desired goal is to obtain a simultaneous good fit for all reactions, that is, to minimize all SRS_i. This constitutes a multi-objective optimization problem. The proposed objective function was the total weighted sum of residual squares (*TWSRS*) defined by Eq. 11, by selecting appropriate scalar weights, w_i.

$$TWSRS = \sum_{i=1}^{r} w_i \cdot SRS_i = \sum_{i=1}^{r} w_i \left(r_i^{\exp} - r_i^{calc} \right)^2 \qquad (11)$$

It can be difficult to discern how to set the weights for compensating the differences in individual objective function magnitudes (SRS_i), because measured reaction rates differ from one reaction to other. If $w_i=1$ is selected, that is equal importance for all responses, the obtained solution fits relatively better for large reaction rate values; if $w_i=1/(r_i^{exp})^2$, the procedure gives priority to the fitting of low reaction rates. However, if each objective function is divided by their respective maxima, objective functions are normalized between zero and one and then similar importance can be given to all objective functions minimized [40]. Consequently, the selected weights were $w_i=1/(r^{exp}_{i,max})^2$. A MATLAB script that applies the Levenberg-Marquardt method [41] was developed to estimate the kinetic parameters by minimizing *TWSRS*.

3.5.2.5 Criteria for model selection and model averaging

A suitable model has to predict accurately the experimental evolution of the composition of reaction medium in every single experimental run, all included parameters being relevant, and the estimated parameter values must present coherent thermodynamic and kinetic meaning. To

discriminate among the different kinetic models, several criteria have been adopted, where a model is rejected if the fitted parameter values, or their estimated error, falls outside of a certain range. The considered ranges have been taken as very wide to be conservative, mainly to avoid the wrong rejection of a good candidate model, because the fit of reaction rates equations is a clearly nonlinear problem and, therefore, parameters can be highly crosscorrelated and non-normally distributed.

The first applied criteria was purely mathematic: models that present at least one fitted parameter with an estimated error larger than 3-fold its parameter value were directly rejected, because it indicates that the effect of the parameter is very likely non-significant. The parameter error value has been estimated as the square root of the diagonal elements from the covariance matrix of parameter estimates.

Parameters $K_{1,j}$ and $K_{T,j}$ are related to adsorption enthalpy and entropy of species *j* on the catalyst (Eq. 8). For a candidate model, their values, and taking into account the parameter uncertainty, have to fulfill the Boudart rules [42]:

i) $\Delta_{ads}S°_j < 0$, because the adsorption process implies a loss of entropy.
ii) $|\Delta_{ads}S°_j| < S°_j$, because the loss of entropy cannot be larger than the total entropy.
iii) $\Delta_{ads}H°_j < 0$, because adsorption is an exothermic process.

With respect to the apparent kinetic constant, the $k_{T,i}$ parameter (Eq. 9) is related to the apparent activation energy: $k_{T,i} = -E'_{a,i}/\mathrm{R}$. Kinetic models where the obtained apparent activation energy for at least one reaction was either larger than 300 kJ/mol (an extremely large value for R1-R4 reactions [43]), or negative, were discarded.

The traditional approach to choose the best model is to select the one providing the highest prediction ability of experimental data with the lower number of parameters. But this approach ignores uncertainty in model selection. Several models can describe experimental data satisfactorily and it is hard to discriminate among them to find the true model, because the models ranked in the group of best models are expected to be similar, and the experimental error can mask which is the true model. The concept of model averaging stems for the choice of a weighted average of the estimates obtained for the group of candidate models, as being more representative of the true values, rather than the choice of the particular estimates obtained for a selected model. The candidate models are those that present coherent thermodynamical meaning of the parameters and with lower deviation with respect experimental data. For this group composed of *M* candidate kinetic models, several criteria can be applied for model selection and averaging, such as the Akaike Information Criterion (AIC) and Bayesian Information Criterion

(BIC) [19–24]. AIC and BIC criteria are useful for penalizing overparameterized models. The Akaike Information Criterion coefficient, *AIC*, can be calculated for each model by the following equation [22]:

$$AIC = N \cdot \ln\left(\frac{TWSRS}{N}\right) + 2(p+1) + \frac{2(p+1)(p+2)}{N-p-2} \tag{12}$$

where N is the number of considered experimental values, and p is the number of parameters. In order to compare among candidate models, the delta *AIC* (Δ_m) and the Akaike weights (AW_m) for each model m are used:

$$\Delta_m = AIC_m - minAIC \tag{13}$$

$$AW_m = \frac{\exp(-\Delta_m/2)}{\sum_{m=1}^{M}\exp(-\Delta_m/2)} \tag{14}$$

where *minAIC* is the minimum value of the *AIC* for the set M of selected models.

The lower the Δ_m value, the more likely model m is the best model [22]. The Akaike weights indicate the probability of a model m to be the best among the group of M selected models. The sum of Akaike weights for the group of candidate models is equal to unity. Finally, natural model averaging [19,20,24] can be applied to the candidate models to calculate the weighted average of each parameter, θ, by means of the following equation:

$$\theta = \sum_{m=1}^{M} AW_m \theta_m \tag{15}$$

where θ_m is the value of the parameter estimate for model m from the group of M selected models.

3.5.2.6 Modeling results

Considering all the possible variations for each term of general Eq. 3, a total of 3,076 possible combinations (models) were obtained for each n (1, 2 or 3), which results in a total of 9,228 kinetic models. These combinations can be divided into two different sets or families of models: those that consider the fraction of free active sites significant (set I) and those that consider saturated the catalytic surface (set II). Table 2 shows the complete form of rate equations for these two sets. K'_k and k'_i for equations in set II are, in fact, K_k/K_j and k_i/K_j, respectively.

Table 2

It was found that the simultaneous fit of r_{R1}, r_{R2}, r_{R3} and r_{R4} was unachievable to perform, because of the extremely large error obtained for the estimates of the isoamylenes isomerization reaction (R4). This can be attributed to the proximity of the IA mixture to the isomerization equilibrium along the experimental runs. Therefore, the variation of the relative amounts between 2M1B and 2M2B during the runs was very low, what did not enable the simultaneous estimation of all the reactions studied. A similar drawback had been observed by Linnekoski et al. [44] and by Rihko et al. [45] in the kinetic modeling of the etherification of IA with EtOH and methanol (MeOH), respectively. Due to the low progress of the isomerization reaction, only r_{R1}, r_{R2} and r_{R3} were considered in the simultaneous fitting procedure. The results obtained after such decision confirmed the correct optimization and estimation of parameters for the fitted kinetic models.

It has been reported that the fraction of free active sites (α=1) is only relevant for alcohol molar fractions lower than 0.04 [43]. In the present work, EtOH concentration was higher. However, models from set I were not discarded to verify this assumption. Indeed, results showed that Boudart rules were not fulfilled for most of the models from set I, because positive values for the enthalpy of adsorption of involved compounds were obtained. Where Boudart rules were fulfilled, the values of *TWSRS* were considerably larger than those obtained for models from set II (α=0). As a consequence, it can be assumed that the fraction of unoccupied active sites is very low and, therefore, equations of set II are more appropriate to describe the reaction system. The obtained values of estimates for the first five ranked best models are gathered in Tables 3, 4 and 5 for n=1, 2 and 3, respectively. All models in these tables belong to set II equations, with the common characteristic that the first summand of the adsorption term, which is not accompanied by a parameter to be fitted, is the ethanol activity, a_{EtOH}. They provided a good fit, with thermodynamic coherence of the parameter estimates and with a low associated error.

Table 3

Table 4

Table 5

Globally, it can be seen that the values of *TWSRS* and *AIC* are similar for the best models with n = 1 and n = 2, and, therefore, it is difficult to discern which value of n is more appropriate. On the other side, models with n = 3 present notably larger values of *TWSRS* and *AIC*, what suggests that the participation of three active sites in the etherification reactions (R1 to R3) is not likely to occur.

From the analysis of the obtained results, some common features have been observed between the best models:

i) There is a coincidence of the form of the best models for $n = 1$ and $n = 2$. They include the contribution of the same species in the adsorption term, the main differences being whether the temperature dependence of this contribution is significant or not. Moreover, the range of variation of the estimates obtained for different models was quite narrow, which is definitely a trustworthy sign of the reliability of the estimated values and the similarity of the best models, what supports the adequacy of the model averaging procedure.

ii) EtOH adsorption was significant in all the best models. Since it appeared as the first summand of the adsorption term, the adsorption equilibrium constants of the rest of adsorbed species j are, in fact, $K'_j = K_j/K_{EtOH}$.

iii) ETBE adsorption was always significant, since $K'_{1,ETBE}$ appeared in all the best models, and its temperature dependent parameter, $K'_{T,ETBE}$, appeared in about the half of the best models. Therefore, K'_{ETBE} has been considered as temperature dependent.

iv) TAEE adsorption contributed in some of the candidate models, and its temperature dependent term was rarely significant. K'_{TAEE} has been considered as constant within the assayed temperature range.

v) Olefins (IB, 2M1B, and 2M2B) adsorption contribution did not appear in the best kinetic models, what indicates that their adsorption is negligible under the explored conditions.

vi) The solubility parameter of Amberlyst™ 35, δ_p, and hence the resin-medium affinity factor, ψ, was included in almost all the best models, what indicates that the catalyst activity is affected by this interaction. Since its temperature dependent term (k_{DT}) was only significant in few candidate models, δ_p has been considered as constant within the assayed range of temperature. For models were k_{DT} was significant, its value was lower than 0.1 $MPa^{1/2}K^{-1}$, which is comparable with that determined in previous kinetic studies using a similar catalyst [14].

As a basis of the common features observed in the best models, the model averaging procedure has been applied to estimate the parameter values and their uncertainty in order to propose a reliable kinetic model. The results are gathered in Table 6.

Table 6

As it can be seen, *TWSRS* values from model averaging almost match the lowest values for the best individual models with n=1, 2, and 3 (Tables 3, 4 and 5). The magnitude of fitted

parameters and associated error obtained after model averaging are acceptable. Consequently, such estimated values can be considered as more representative of the true values than for an individual model, since they incorporate balanced information about the set of best selected models, and the model uncertainty has been also taken into account.

On one hand, lower similar values of *TWSRS* were obtained for n=1 and n=2, but there is not a clear evidence for discriminating between them beyond a doubt. On the other hand, in previous published studies, the proposed number of active sites for the isolated synthesis of ETBE and TAEE was typically 2 or 3 [43], that is, the participation of two active sites seems more feasible rather than only one. Finally, estimated values of K'_{ETBE} and K'_{TAEE} are lower for n=2 than for n=1, and generally lower that unity, as expected in a preferential adsorption of EtOH compared to ethers, because of its higher polarity [15]. Based upon these reasons, the averaged model model with n=2 was selected as the more reliable for the present reaction system. Eqs. 16 and 17 are the finally proposed kinetic equations obtained for ETBE and TAEE formation. Fig. 6 shows the comparison of predicted vs experimental reaction rates from Eqs. 16 and 17.

$$r_{ETBE} = r_{R1} = \frac{k'_{R1}\left(a_{IB}a_{EtOH} - a_{ETBE}/K_{R1}\right)\psi}{\left(a_{EtOH} + K'_{ETBE}\,a_{ETBE} + K'_{TAEE}\,a_{TAEE}\right)^2} \tag{16}$$

$$r_{TAEE} = r_{R2} + r_{R3} = \frac{\left[k'_{R2}\left(a_{2M1B}a_{EtOH} - a_{TAEE}/K_{R2}\right) + k'_{R3}\left(a_{2M2B}a_{EtOH} - a_{TAEE}/K_{R3}\right)\right]\psi}{\left(a_{EtOH} + K'_{ETBE}\,a_{ETBE} + K'_{TAEE}\,a_{TAEE}\right)^2} \tag{17}$$

Figure 6

Parameters appearing in the adsorption term, K'_j, are not the actual adsorption equilibrium constant of species j, but K_j/K_{EtOH} ratios. For ETBE, estimated K_{ETBE}/K_{EtOH} values ranged from 0.47 at 323 K to 1.55 at 353 K. Such increase suggests that ETBE adsorption is gaining relevance with temperature, compared to EtOH adsorption. For TAEE, a constant value of 0.48 was obtained for K_{TAEE}/K_{EtOH} within the explored range of temperature. This value is very similar to that of ETBE at 323 K indicating that adsorption equilibrium constants of both ethers are comparable at low temperature. Some thermodynamic information can be obtained from the ratio of adsorption equilibrium constants, K'_j, according to Eq. 18. Estimated differences of adsorption enthalpies and entropies resulted in $(\Delta_{ads}H^o_{ETBE,(l)} - \Delta_{ads}H^o_{EtOH,(l)})$=37.9 kJ/mol, and $(\Delta_{ads}S^o_{ETBE,(l)} - \Delta_{ads}S^o_{EtOH,(l)})$= –0.97 J/(mol·K). These results indicate that EtOH adsorption is more exothermic than adsorption of ETBE and that the entropic loss for the adsorbed EtOH is larger than for the adsorbed ETBE. With respect to the adsorption Gibbs free energy difference between ETBE and EtOH $(\Delta_{ads}G^o_{ETBE,(l)} - \Delta_{ads}G^o_{EtOH,(l)})$ varied from 2.04 kJ/mol at 323 K to –1.29

kJ/mol at 353 K, and a constant difference value ($\Delta_{ads}G^{o}_{TAEE,(l)}-\Delta_{ads}G^{o}_{EtOH,(l)}$)=1.98 kJ/mol was estimated between TAEE and EtOH adsorption. On one side, EtOH adsorption seems to be more favored than ETBE adsorption at low temperature, and less favored at high temperature, and, on the other, TAEE adsorption would be less favored than EtOH adsorption within the whole temperature range.

$$K_j' = \frac{K_j}{K_{EtOH}} = \exp\left(K'_{1,j} + K'_{T,j}\left(\frac{1}{T}-\frac{1}{\overline{T}}\right)\right) = \exp\left(\frac{\Delta_{ads}S^{\circ}_{j,(l)} - \Delta_{ads}S^{\circ}_{EtOH,(l)}}{R} - \frac{\Delta_{ads}H^{\circ}_{j,(l)} - \Delta_{ads}H^{\circ}_{EtOH,(l)}}{R}\left(\frac{1}{T}-\frac{1}{\overline{T}}\right)\right) = \\ = \exp\left(\frac{-\left(\Delta_{ads}G^{\circ}_{j,(l)} - \Delta_{ads}G^{\circ}_{EtOH,(l)}\right)}{R}\left(\frac{1}{T}-\frac{1}{\overline{T}}\right)\right) \quad (18)$$

With respect to the estimates of the resin solubility parameter, δ_p, they ranged from 17 to 30 $MPa^{1/2}$ for the whole set of candidate models. The value for the final averaged model (n=2) is 21.16±0.12 $MPa^{1/2}$ as a mean value within 323-353 K. This result is in good agreement with the constant value of 20.9±2.0 $MPa^{1/2}$ from 313 to 353K proposed by González [28] for A-35 in the isolated liquid-phase synthesis of ETBE, which gives reliability to the proposed kinetic models in this study.

Once the final kinetic equations for R1, R2 and R3 (Eqs. 16 and 17) and their parameters were determined, the kinetic parameters of isoamylenes isomerization, R4, have been estimated. In that case, a separated non-linear least squares minimization was performed using the estimates previously obtained for n=2 (Table 6). The kinetic term k'_{R4} comprised the only two parameters to be estimated. It was found that optimization could be satisfactorily performed and the best results in terms of lower sum of squares indicated that one active site is involved in isoamylenes isomerization reaction, in accordance with a unimolecular reaction. The values obtained for the estimates $k'_{1,R4}$ and $k'_{T,R4}$ were 6.27 and –9199 K, respectively, and consequently an apparent activation energy of 76.5 kJ/mol. The proposed kinetic expression for the isoamylenes double bond isomerization is shown in Eq. 19. Although these obtained values are considered as approximate estimates, they are consistent with values quoted in previous studies [9, 29].

$$r_{2M2B} = r_{R4} - r_{R3} = \frac{\left[k'_{R4}(a_{2M1B} - a_{2M2B}/K_{R4}) - k'_{R3}(a_{2M2B}a_{EtOH} - a_{TAEE}/K_{R3})\right]\psi}{\left(a_{EtOH} + K'_{ETBE}\,a_{ETBE} + K'_{TAEE}\,a_{TAEE}\right)} \quad (19)$$

The values of apparent activation energies ($E'_{a,i}$) for reactions R1 to R4, and their associated standard error, obtained with the averaged model are gathered in Table 7, and compared with published values for the isolated synthesis of ETBE and TAEE over similar catalysts. In etherification reactions, $E'_{a,i}$ was found to increase as the exothermicity of reaction decreases, that is in the order R1< R2 < R3. $E'_{a,R1}$ is in good agreement with published values in the

synthesis of ETBE over Amberlyst™ 15 by Ancillotti et al. [46], and over Amberlyst™ 35 by Gonzalez [28]. $E'_{a,R2}$ and $E'_{a,R3}$ are in reasonable agreement with those determined by Linnekoski et al. [9] in the synthesis of TAEE over Amberlyst™ 16. $E'_{a,R4}$ value is in fair agreement with the values of 72.9 and 91 kJ/mol for IA isomerization over Amberlyst™ 16 proposed by Linnekoski et al. [9,29]. Generally, published $E'_{a,i}$ values shown in Table 7, obtained with similar resins, are slightly higher than those obtained in this work, what indicates a lower temperature sensitivity of A-35 compared to the other resins. A few values of $E'_{a,i}$ presented in Table 7 using resins with commercial bead size are rather low, within the range 40-55 kJ/mol, probably due to the presence of internal diffusion effects.

Table 7

The apparent rate coefficient is related with the reactivity of olefins with EtOH. Fig. 7 shows the Arrhenius plot of the kinetic constant obtained for every reaction. Olefins reactivity in etherification with EtOH follows the order 2M1B>IB>2M2B, what indicates that a terminal double bond (α-position, 2M1B) reacts more readily than an internal double bond (β-position, 2M2B). Rihko et al. [50] also observed a higher reactivity for 2M1B than for 2M2B in the isolated etherification of IA with EtOH. Since both IA form the same carbocation, differences in their reactivity can be explained by an easier protonation of the terminal double bond due to a lower steric hindrance.

Figure 7

Some outcomes about the reacting process are derived from kinetic equations 16, 17, and 19. The form of the driving force term indicates that the surface reaction is the rate-determining step for all reactions. The inclusion of the ψ factor shows that the interaction between the reaction medium and the resin affects the catalytic activity. Species appearing in the adsorption term, namely EtOH, ETBE, and TAEE, are those adsorbed onto the catalytic active sites, and olefins do not adsorb in a significant extent. Finally, two active sites participate in the rate-determining step, the surface reaction, in etherification reactions, and one active site in IA isomerization.

The proposed kinetic equations can come from either a LHHW o an ER mechanism. A LHHW mechanism involves that all species taking part in the surface reaction are adsorbed on the catalyst. In an ER mechanism at least one of the species is not adsorbed and it reacts directly from the reaction medium with other adsorbed species. Since alcohols are preferentially adsorbed on the active sites compared to olefins, as quoted in literature [15] and enforced by the results of this study, in case of the etherification through an ER mechanism it is more likely that olefins react directly from the reaction medium. This is not in contradiction that olefins adsorb

on the resin, but more weakly, as seen that isomerization also occurs on the active sites. For comparable isolated etherification systems, Tejero et al. [51] and Françoise and Thyrion [8] suggested a transition from ER mechanisms to LHHW when the alcohol concentration become very low. Nonetheless, this transition of mechanisms is unexpected in the present work, because EtOH molar fraction was always higher than 0.04, and, therefore, an ER mechanism seems to be more reasonable.

In the reaction rate equations, the main difference between a LHHW and an ER mechanisms is the form of the kinetic term. Considering the surface reaction between one molecule of alcohol and one molecule of olefin as the rate-determining step, the corresponding kinetic term for a LHHW is expressed as $k_i=k^*_i\, K_{olefin}\, K_{alcohol}$, where k^*_i is the intrinsic kinetic constant, whereas for an ER mechanism it is $k_i=k^*_i\, K_{alcohol}$. Besides, for models that consider negligible the fraction of free active sites (set II), these kinetic terms vary depending upon the form of the adsorption term and the number of involved active sites. Hence, the kinetic terms of Eqs. 16 and 17 are expressed as: $k'_i=k^*_i\, K_{olefin}/K_{alcohol}$ for a LHHW mechanism or $k'_i=k^*_i/K_{alcohol}$ for an ER one. As a result, the true activation energies ($E_{a,i}$) of etherification reactions can be calculated from apparent activation energies ($E'_{a,i}$) and liquid-phase adsorption enthalpies ($\Delta_{ads}H^o_{j,(l)}$) of reactants as $E_{a,i} = E'_{a,i} - \Delta_{ads}H^o_{olefin,(l)} + \Delta_{ads}H^o_{alcohol,(l)}$ for a LHHW mechanism, or as $E_{a,i} = E'_{a,i} + \Delta_{ads}H^o_{alcohol,(l)}$ for an ER mechanism. If not available, liquid-phase adsorption enthalpy can be estimated from the sum of the gas-phase adsorption enthalpy ($\Delta_{ads}H^o_{j,(g)}$) and the enthalpy of vaporization of compound ($\Delta_vH^o_j$). It is to be noted that an important lack of agreement between sources was found in the literature for thermodynamic adsorption properties of reactants. This divergence affects to the calculation of $E_{a,i}$. As no data were available for adsorption thermodynamic properties of EtOH and olefins on A-35, experimentally gas-phase determined values over Amberlyst™ 15, which is similar to Amberlyst™ 35 but with lower acid capacity, were used instead (Table 8). The resulting true activation energies estimated for LHHW or ER mechanisms, are gathered in Table 9.

Table 8

Table 9

The true activation energies values determined for the LHHW mechanism shown in Table 9 seem unlikely, since they are too high compared to values reported in the literature for isolated etherification of IB and IA with EtOH over similar catalysts [7,9]. So it can be concluded that an ER mechanism, in which adsorbed EtOH reacts with non-adsorbed olefins, is the most likely for the studied etherification reactions. The choice of an ER mechanism as the most feasible is

in concordance with the results obtained from non-linear regression, which suggested one or two active sites as the most probable and with previous kinetic studies on the isolated etherification of isoalkenes with primary alcohols [7,11,51]. With respect to isoamylenes double bond isomerization reaction between the α- and the β-position of the alkenes [50], it follows an LHHW mechanism in which an adsorbed molecule of 2M1B (more reactive and less thermodynamically stable than 2M2B) adsorbs on one active site to form 2M2B.

To sum up, taking into account the complexity of the studied system with three etherification reactions and one double bond isomerization that occur simultaneously, the proposed kinetic model can be considered as appropriate and reliable for describing the experimental runs. Results are coherent with previous studies on kinetics of isolated tertiary ether syntheses. Finally, additional experimental determination of liquid- and gas-phase adsorption thermodynamic properties of involved compounds on A-35 would provide valuable information for a categorical description of the actual reaction mechanisms and possible mechanism transition under different conditions.

4. Conclusions

The simultaneous etherification of isobutene (IB) and isoamylenes (2M1B and 2M2B) with ethanol (EtOH) has been carried out at 323–353K and catalyzed by Amberlyst™ 35. The involved reactions are ethyl *tert*-butyl ether (ETBE) and *tert*-amyl ethyl ether (TAEE) formation, and also double bond isomerization between 2M1B and 2M2B. Formation rate of ETBE is faster than global formation rate of TAEE. A large number of kinetic equations, expressed in terms of activities and based on the LHHW–ER formalism, have been systematically proposed and fitted to experimental data to obtain satisfactory kinetic models for the whole reaction network. Model selection and model averaging have been shown as a convenient technique to obtain a reliable kinetic model. The best obtained model in etherification stems for the surface reaction between one molecule of alcohol and one of olefin with the participation of two active sites. Adsorption of EtOH, ETBE and TAEE is significant, and the fraction of non-occupied sites is negligible. Obtained results confirmed that adsorption of EtOH is stronger than that of olefins. EtOH is preferentially adsorbed rather than TAEE within the explored temperature and its adsorption is also favored compared to ETBE only at low temperatures. One active site participates in isoamylenes double bond isomerization. Apparent activation energies for ETBE formation from IB and EtOH, TAEE formation from 2M1B and EtOH, TAEE formation from 2M2B and EtOH, and isoamylenes double bond isomerization were 72.8±1.4, 74.9±2.8, 81.2±2.2 and, 76.5±7.2 kJ/mol, respectively. These values are in good agreement with those quoted in literature for the isolated ETBE and TAEE

formation systems. 2M1B has been found to be more reactive with EtOH than 2M2B. From the estimated activation energies values, it has been found that an Eley-Rideal mechanism is more likely to occur than a LHHW mechanism in the etherification reactions.

Acknowledgments

The authors are grateful to Rohm & Haas France SAS (The Dow Chemical Company) for providing the ion-exchange resin Amberlyst™ 35 used in this work.

Notation

$\Delta_{ads}G^o$	standard molar Gibbs free energy of adsorption [kJ·mol^{-1}]
$\Delta_{ads}H^o$	standard molar enthalpy of adsorption [kJ·mol^{-1}]
$\Delta_{ads}S^o$	standard molar entropy of adsorption [J·mol^{-1}·K^{-1}]
2M1B	2-methyl-1-butene
2M2B	2-methyl-2-butene
a	activity of chemical compound
AIC	Akaike Information Criterion coefficient
AW_m	Akaike weight of model m
DF	driving force
d_p	particle diameter [mm]
ETBE	ethyl *tert*-butyl ether
IA	isoamylenes
IB	isobutene
K_i	equilibrium constant of reaction i [dimensionless]
K_j	adsorption equilibrium constant of compound j [dimensionless]
k^*_i	intrinsic kinetic coefficient of reaction i [mol·h^{-1}·kg$_{cat}^{-1}$]
k'_i	apparent kinetic coefficient of reaction i [mol·h^{-1}·kg$_{cat}^{-1}$]
k_i	apparent kinetic coefficient of reaction i [mol·h^{-1}·kg$_{cat}^{-1}$]
M	set of candidate models
N	sample size, number of experimental points

n number of active sites or clusters of active sites participating in the rate-determining step

p number of parameters of the model

R gas constant, 8.314472 $J \cdot mol^{-1} \cdot K^{-1}$

r^0_j initial formation rate of compound j [$mol \cdot h^{-1} \cdot kg_{cat}^{-1}$]

r_j formation rate of compound j [$mol \cdot h^{-1} \cdot kg_{cat}^{-1}$]

$R^o_{A/O}$ initial molar ratio of alcohol to olefins

$R^o_{C4/C5}$ initial molar ratio of isobutene to isoamylenes

SRS sum of squares of residuals

T temperature [K]

TAA *tert*-amyl alcohol

TAEE *tert*-amyl ethyl ether

TBA *tert*-butyl alcohol

TWSRS total weighted sum of residuals squares

W_{cat} catalyst mass in dry basis [g]

w_i weight assigned to each objective function

Greek letters

α parameter that takes the value of either unity or zero.

Δ_m delta of Akaike for model m

δ Hildebrand solubility parameter [$MPa^{1/2}$]

ψ resin-medium affinity factor [dimensionless]

θ estimate value

Subscripts

(g) gas-phase

(l) liquid-phase

1 temperature independent term

i reaction

j	chemical compound
k	chemical compound different than *j*
m	number of model considered
p	related to the polymer (catalyst)
T	temperature dependent term
v	vaporization

Superscripts

0	Initial
S	total number of compounds
exp	experimental
calc	calculated

References

[1] T. Zhang, K. Jensen, P. Kitchaiya, C. Phillips, R. Datta, Liquid-phase synthesis of ethanol-derived mixed tertiary alkyl ethyl ethers in an isothermal integral packed-bed reactor, Ind. Eng. Chem. Res. 36 (1997) 4586–4594.

[2] C. Gómez, F. Cunill, M. Iborra, J.F. Izquierdo, J. Tejero, Experimental study of the simultaneous synthesis of methyl tert-butyl ether and ethyl tert-butyl ether in liquid phase, Ind. Eng. Chem. Res. 36 (1997) 4756–4762.

[3] R. Soto, C. Fité, E. Ramírez, R. Bringué, M. Iborra, Green metrics analysis applied to the simultaneous liquid-phase etherification of isobutene and isoamylenes with ethanol over Amberlyst™ 35, Green Process. Synth. 3 (2014) 321–333.

[4] R. Soto, C. Fité, E. Ramírez, J. Tejero, F. Cunill, Effect of water addition on the simultaneous liquid-phase etherification of isobutene and isoamylenes with ethanol over Amberlyst™ 35, Catal. Today. 256 (2015) 336–346.

[5] R. Soto, C. Fité, E. Ramírez, R. Bringué, F. Cunill, Equilibrium of the simultaneous etherification of isobutene and isoamylenes with ethanol in liquid-phase, Chem. Eng. Res. Des. 92 (2014) 644–656.

[6] R. Soto, C. Fité, E. Ramírez, R. Bringué, F. Cunill, Equilibrium conversion, selectivity and yield optimization of the simultaneous liquid-phase etherification of isobutene and isoamylenes with ethanol over Amberlyst™ 35, Fuel Process. Technol. 142 (2016) 201–211.

[7] C. Fité, M. Iborra, J. Tejero, J.F. Izquierdo, F. Cunill, Kinetics of the liquid-phase synthesis of ethyl tert-butyl ether (ETBE), Ind. Eng. Chem. Res. 33 (1994) 581–591.

[8] O. Françoisse, F.C. Thyrion, Kinetics and mechanism of ethyl tert-butyl ether liquid-phase synthesis, Chem. Eng. Process. Process Intensif. 30 (1991) 141–149.

[9] J.A. Linnekoski, A.O. I. Krause, L. Rihko. Kinetics of the heterogeneously catalyzed formation of tert-amyl ethyl ether, Ind. Eng. Chem. Res. 36 (1997) 310–316.

[10] N. Oktar, K. Mürtezaoğlu, G. Doğu, I. Gönderten, T. Doğu, Etherification rates of 2-methyl-2-butene and 2-methyl-1-butene with ethanol for environmentally clean gasoline production, J. Chem. Technol. Biotechnol. 74 (1999) 155–161.

[11] L. Rihko-Struckmann, P.V. Latostenmaa, A.O. Krause, Interaction between the reaction medium and an ion-exchange resin catalyst in the etherification of isoamylenes, J. Mol. Catal. A Chem. 177 (2001) 41–47.

[12] M.S. Caceci, Estimating error limits in parametric curve fitting, Anal. Chem. 61 (1989) 2324–2327.

[13] C. Fité, J. Tejero, M. Iborra, F. Cunill, J.F. Izquierdo, D. Parra, The effect of the reaction medium on the kinetics of the liquid-phase addition of methanol to isobutene, Appl. Catal. A Gen. 169 (1998) 165–177.

[14] C. Fité, J. Tejero, M. Iborra, F. Cunill, J.F. Izquierdo, Enhancing MTBE rate equation by considering reaction medium influence, AIChE J. 44 (1998) 2273–2279.

[15] N. Oktar, K. Mürtezaoğlu, G. Doğu, T. Doğu, Dynamic analysis of adsorption equilibrium and rate parameters of reactants and products in MTBE, ETBE and TAME production, Can. J. Chem. Eng. 77 (1999) 406–412.

[16] K.F. Yee, A.R. Mohamed, S.H. Tan, A review on the evolution of ethyl tert-butyl ether (ETBE) and its future prospects, Renew. Sustain. Energy Rev. 22 (2013) 604–620.

[17] G. Bozga, A. Motelica, R. Dima, V. Plesu, A. Toma, C. Simion, Evaluation of published kinetic models for tert-amyl ethyl ether synthesis, Chem. Eng. Process. Process Intensif. 47 (2008) 2247–2255.

[18] European Fuel Oxygenates Association (EFOA). http://www.efoa.eu/ (accessed January, 2016).

[19] F.E. Turkheimer, R. Hinz, V.J. Cunningham, On the undecidability among kinetic models: from model selection to model averaging, J. Cereb. Blood Flow Metab. 23 (2003) 490–498.

[20] L. Wasserman, Bayesian model selection and model averaging, J. Math. Psychol. 44 (2000) 92–107.

[21] J.A. Hoeting, D. Madigan, A.E. Raftery, C.T. Volinsky, Bayesian model averaging: a tutorial, Stat. Sci. 14 (1999) 382–417.

[22] G. Glatting, P. Kletting, S.N. Reske, K. Hohl, C. Ring, Choosing the optimal fit function: comparison of the Akaike information criterion and the F-test., Med. Phys. 34 (2007) 4285–4292.

[23] K.P. Burnham, D.R. Anderson, Model selection and multimodel Inference: A Practical Information-Theoretic Approach, second ed. Springer Science, New York, 2003.

[24] M.R.E. Symonds, A. Moussalli, A brief guide to model selection, multimodel inference and model averaging in behavioural ecology using Akaike's information criterion, Behav. Ecol. Sociobiol. 65 (2010) 13–21.

[25] J.H. Badia, C. Fité, R. Bringué, M. Iborra, F. Cunill, Catalytic activity and accessibility of acidic ion-exchange resins in liquid phase etherification reactions, Top. Catal. 58 (2015) 919–932.

[26] F. Aiouache, S. Goto, Sorption effect on kinetics of etherification of tert-amyl alcohol and ethanol, Chem. Eng. Sci. 58 (2003) 2065–2077.

[27] M. Umar, A.R. Saleemi, S. Qaiser, Synthesis of ethyl tert-butyl ether with tert-butyl alcohol and ethanol on various ion exchange resin catalysts, Catal. Commun. 9 (2008) 721–727.

[28] R. González, Performance of Amberlyst™ 35 in the synthesis of ETBE from ethanol and C4 cuts, PhD Thesis, University of Barcelona, 2011.

[29] J.A. Linnekoski, P. Kiviranta-Pääkkönen, A.O. Krause, L. Rihko-Struckmann, Simultaneous isomerization and etherification of isoamylenes, Ind. Eng. Chem. Res. 38 (1999) 4563–4570.

[30] F. Ancillotti, M.M. Mauri, E. Pescarollo, L. Romagnoni, Mechanism in the reaction between olefins and alcohols. J. Mol. Catal. 4 (1978) 37-48.

[31] J. Gmehling, J. Li, M. Schiller, A modified UNIFAC model. 2. Present parameter matrix and results for different thermodynamic properties, Ind. Eng. Chem. Res. 32 (1993) 178–193.

[32] J. Gmehling, J. Lohmann, A. Jakob, J. Li, R. Joh, A modified UNIFAC (Dortmund) model. 3. Revision and extension, Ind. Eng. Chem. Res. 37 (1998) 4876–4882.

[33] J. Lohmann, R. Joh, J. Gmehling, From UNIFAC to modified UNIFAC (Dortmund), Ind. Eng. Chem. Res. 40 (2001) 957–964.

[34] L. Solà, M.A. Pericàs, F. Cunill, J. Tejero, Thermodynamic and kinetic studies of the liquid phase synthesis of tert-butyl ethyl ether using a reaction calorimeter, Ind. Eng. Chem. Res. 34 (1995) 3718–3725.

[35] M.V. Ferreira, J.M. Loureiro, Number of actives sites in TAME synthesis: mechanism and kinetic modeling, Ind. Eng. Chem. Res. 43 (2004) 5156–5165.

[36] R. C. Reid, J.M. Prausnitz, B.E.Poiling, The properties of gases and liquids, fourth ed., Mc Graw Hill, New York, 1987.

[37] J. Guilera, Ethyl octyl ether synthesis from 1-octanol and ethanol or diethyl carbonate on acidic ion- exchange resins, PhD Thesis, University of Barcelona, 2013.

[38] C. Reichardt, Solvents and solvent effects in organic chemistry, third ed., Willey-VCH, Weinheim, 2003, pp.9, 220.

[39] C.L. Yaws, Thermophysical properties of chemicals and hydrocarbons, second ed., Elsevier Science, Oxford, 2014, pp. 366 -489.

[40] R.T. Marler, J.S. Arora, The weighted sum method for multi-objective optimization: new insights, Struct. Multidisc. Optim. 41 (2010) 853–862.

[41] G. Puxty, M. Maeder, K. Hungerbühler, Tutorial on the fitting of kinetics models to multivariate spectroscopic measurements with non-linear least-squares regression, Chemom. Intell. Lab. Syst. 81 (2006) 149–164.

[42] M. Boudart, D.E. Mears, M.A Vannice. Kinetics of heterogeneous catalytic reactions, Ind. Chim. Belge. 32 (1967) 281-284.

[43] H. Hamid, M.A. Ali, Handbook of MTBE and other gasoline oxygenates, Marcel Dekker, Inc., New York, 2004.

[44] J.A. Linnekoski, A.O. Krause, L.K. Struckmann, Etherification and hydration of isoamylenes with ion exchange resin, Appl. Catal. A Gen. 170 (1998) 117–126.

[45] L.K. Rihko, P.K. Kiviranta-Pääkkönen, A.O. Krause, Kinetic model for the etherification of isoamylenes with methanol, Ind. Eng. Chem. Res. 36 (1997) 614–621.

[46] F. Ancillotti, M.M. Mauri, E. Pescarollo, Ion exchange resins catalyzed addition of alcohols to olefins, J. Catal. 46 (1977) 49-57.

[47] M. Umar, D. Patel, B. Saha, Kinetic studies of liquid phase ethyl tert-butyl ether (ETBE) synthesis using macroporous and gelular ion exchange resin catalysts, Chem. Eng. Sci. 64 (2009) 4424–4432.

[48] B.-L. Yang, S. B. Yang, R. Yao, Synthesis of ethyl tert-butyl ether from tert-butyl alcohol and ethanol on strong acid cation-exchange resins, React. Funct. Polym. 44 (2000) 167–175.

[49] O. Boonthamtirawuti, W. Kiatkittipong, A. Arpornwichanop, P. Praserthdam, S. Assabumrungrat, Kinetics of liquid phase synthesis of tert-amyl ethyl ether from tert-amyl alcohol and ethanol over Amberlyst 16, J. Ind. Eng. Chem. 15 (2009) 451–457.

[50] L.K. Rihko, A.O.I. Krause, Reactivity of isoamylenes with ethanol, Appl. Catal. A Gen. 101 (1993) 283–295.

[51] J. Tejero, F. Cunill, J.F. Izquierdo, M. Iborra, C. Fité, D. Parra, Scope and limitations of mechanistic inferences from kinetic studies on acidic macroporous resins The MTBE liquid-phase synthesis case, Appl. Catal. A Gen. 134 (1996) 21–36.

[52] R.M. Stephenson, S. Malanowski, Handbook of the thermodynamics of organic compounds. Elsevier, New York, 1987.

[53] P. Słomkiewicz, Determination of the adsorption equilibrium of alcohols and alkenes on a sulphonated styrene–divinylbenzene copolymer, Adsorpt. Sci. Technol. 24 (2006) 239–256.

Tables

Table 1. Experimental reaction rates

T [K]	$R^{o}_{A/O}$	$R^{o}_{C4/C5}$	r^{0}_{EtOH} [mol·(kg$_{cat}$·h)$^{-1}$]	r^{0}_{2M2B} [mol·(kg$_{cat}$·h)$^{-1}$]	r^{0}_{ETBE} [mol·(kg$_{cat}$·h)$^{-1}$]	r^{0}_{TAEE} [mol·(kg$_{cat}$·h)$^{-1}$]	$r^{0}_{ETBE}/r^{0}_{TAEE}$
323.2	1.00	1.00	–153.9	–21.4	122.4	24.8	4.9
323.0	1.99	0.51	–63.1	–20.0	47.7	19.8	2.4
323.1	0.50	0.49	–125.7	–28.2	75.2	38.0	2.0
323.1	0.50	2.02	–265.3	–17.6	244.4	23.9	10.0
323.7	1.99	2.03	–172.8	–14.1	156.0	14.0	11.1
324.7	1.95	2.04	–192.7	–15.0	158.5	15.5	11.1
335.0	1.10	0.99	–379.4	–50.1	299.5	70.1	4.3
333.7	2.06	0.99	–278.5	–28.5	215.8	45.3	4.8
333.7	0.50	0.98	–619.9	–114.4	482.4	130.9	3.7
342.7	1.97	1.00	–522.0	–82.5	422.8	102.4	4.1
345.1	1.01	0.99	–744.6	–128.6	561.5	146.0	3.9
342.7	1.00	1.01	–650.6	–85.8	527.2	130.5	4.0
342.7	0.99	1.03	–660.6	–96.3	525.6	126.6	4.1
342.8	1.00	2.02	–709.5	–69.7	648.6	74.0	8.8
342.8	0.50	1.00	–928.9	–156.3	682.9	176.3	3.9
343.8	0.99	0.50	–627.0	–161.7	432.9	209.3	2.1
353.2	1.97	0.51	–742.4	–188.1	458.6	261.5	1.8
353.5	1.00	1.02	–1765.5	–285.6	1374.6	368.9	3.7
352.7	1.97	2.01	–1096.7	–76.8	946.2	105.7	9.0
352.8	0.50	2.04	–2486.5	–288.8	2207.8	251.4	8.8
353.8	0.50	0.50	–1807.9	–642.3	1126.6	618.1	1.8

Table 2. General form of the considered reaction rate equations. Subscript *i* refer to the chemical reaction, and *j* and *k* to all chemical species adsorbed on the resin active sites.

Set	I	II
Rate equation	$r_i = \dfrac{k_i \{Driving\ force\}_i \psi}{\left(1+\sum_j K_j a_j\right)^{n_i}}$	$r_i = \dfrac{k'_i \{Driving\ force\}_i \psi}{\left(a_j+\sum_{k\neq j} K'_k a_k\right)^{n_i}}$

Table 3. Estimated parameter values for the first five models ranked as best models with *n*=1.

Model	$k'_{1,R1}$	$k'_{T,R1}$	$k'_{1,R2}$	$k'_{T,R2}$	$k'_{1,R3}$	$k'_{T,R3}$	k_{D1}	k_{DT}	$K'_{1,ETBE}$	$K'_{T,ETBE}$	$K'_{1,TAEE}$	$K'_{T,TAEE}$	*TWSRS*	*AIC*
203	6.46	–8954	6.93	–9457	4.59	–9775	23.71	–	0.53	–5139	–	–	0.26	–1193
500	6.47	–8958	7.01	–9781	4.55	–9583	23.68	–	0.41	–5610	–0.41	–	0.26	–1192
104	6.51	–8459	7.03	–7031	4.66	–9849	23.71	–	1.01	–	–	–	0.28	–1185
401	6.51	–8459	7.14	–7236	4.59	–9969	23.67	–	0.94	–	–0.42	–	0.28	–1183
105	6.44	–9119	6.95	–8020	4.59	–10366	24.26	–0.04	1.02	–	–	–	0.28	–1183

Table 4. Estimated parameter values for the first five models ranked as best models with *n*=2.

Model	$k'_{1,R1}$	$k'_{T,R1}$	$k'_{1,R2}$	$k'_{T,R2}$	$k'_{1,R3}$	$k'_{T,R3}$	k_{D1}	k_{DT}	$K'_{1,ETBE}$	$K'_{T,ETBE}$	$K'_{1,TAEE}$	$K'_{T,TAEE}$	*TWSRS*	*AIC*
203	6.42	–8795	6.96	–9035	4.49	–9725	21.18	–	–0.08	–4329	–	–	0.29	–1170
500	6.42	–8795	7.10	–9303	4.39	–9602	21.14	–	–0.24	–4852	–0.74	–	0.30	–1170
401	6.47	–8285	7.26	–6939	4.40	–10138	21.13	–	0.23	–	–0.76	–	0.31	–1160
104	6.47	–8292	7.11	–6674	4.53	–9845	21.17	–	0.34	–	–	–	0.32	–1159
402	6.45	–8497	7.23	–7231	4.38	–10298	21.40	–0.02	0.23	–	–0.75	–	0.31	–1158

Table 5. Estimated parameter values for the first five models ranked as best models with *n*=3.

Model	$k'_{1,R1}$	$k'_{T,R1}$	$k'_{1,R2}$	$k'_{T,R2}$	$k'_{1,R3}$	$k'_{T,R3}$	k_{D1}	k_{DT}	$K'_{1,ETBE}$	$K'_{T,ETBE}$	$K'_{1,TAEE}$	$K'_{T,TAEE}$	*TWSRS*	*AIC*
499	6.28	–9283	7.17	–9607	4.06	–9701	–	–	–0.59	–3849	–0.75	–	0.38	–1122
697	6.30	–9019	7.37	–8178	3.76	–11880	–	–	–0.23	–	–3.47	–25431	0.38	–1122
797	6.26	–8784	7.03	–10026	4.15	–8916	18.46	–	–0.23	–2156	–3.63	–25133	0.38	–1121
500	6.25	–8846	7.05	–9406	4.14	–9373	18.44	–	–0.39	–3709	–0.85	–	0.38	–1120
698	6.28	–8520	7.21	–8742	4.02	–9635	18.46	–	–0.06	–	–3.82	–28586	0.38	–1119

Table 6. Mean values and standard error of the estimates, obtained after model averaging for *n* = 1, 2, and 3.

	n = 1	*n* = 2	*n* = 3
$k'_{1,R1}$	6.47 ± 0.02	6.42 ± 0.02	6.28 ± 0.02
$k'_{T,R1}$	–8950 ± 160	–8760 ± 170	–9000 ± 190
$k'_{1,R2}$	6.96 ± 0.04	7.05 ± 0.04	7.18 ± 0.03
$k'_{T,R2}$	–9520 ± 350	–9010 ± 340	–9150 ± 300
$k'_{1,R3}$	4.58 ± 0.03	4.42 ± 0.03	4.02 ± 0.04
$k'_{T,R3}$	–9720 ± 230	–9770 ± 270	–10150 ± 400
k_{D1}	23.71 ± 0.08	21.16 ± 0.12	–
$K'_{1,ETBE}$	0.50 ± 0.06	–0.12 ± 0.04	–0.35 ± 0.07
$K'_{T,ETBE}$	–5190 ± 480	–4560 ± 410	–3320 ± 440
$K'_{1,TAEE}$	–0.42 ± 0.53	–0.74 ± 0.30	–2.14 ± 0.30
TWSRS	0.26	0.29	0.40

Table 7. Comparison of apparent activation energies obtained in this work with those previously reported for the isolated synthesis of ETBE and TAEE.

Reference	$E'_{a,i}$ [kJ/mol]			Catalyst	Bead size
	ETBE (R1)	TAEE (R2, R3)	Isomerization (R4)		
This work	72.8±1.4	74.9±2.8[a] 81.2±2.2[b]	76.5±7.2	Amberlyst™ 35	0.25–0.4 mm
Ancillotti et al. (1977) [46]	73.8	–	–	Amberlyst™ 15	Commercial
Fité et al. (1994) [7]	86.1	–	–	Bayer K–2631	< 0.1 mm
Solà et al. (1995) [34]	80.6	–	–	Bayer K–2631	0.063–0.16 mm
Umar et al.(2009) [47]	53.46	–	–	Purolite® CT–124	Commercial
Yang et al. (2000) [48]	79.45 43.69 84.11	–	–	Amberlyst™ 15 S–54 D–72	0.7 mm
González (2011) [28]	70.4±3.5	–	–	Amberlyst™ 35	0.25–0.4 mm
Linnekoski et al.(1997) [9]	–	76.8[a] 95.9[b]	72.9	Amberlyst™ 16	0.35–0.65 mm
Linnekoski et al.(1998) [44]	–	88.6	–	Amberlyst™ 16	< 0.65 mm
Linnekoski et al. (1999) [29]	–	87[a] 107[b]	91	Amberlyst™ 16	0.3–0.6 mm
Oktar et al.(1999) [10]	–	40.7[a] 73.6[b]	–	Amberlyst™ 15	Commercial
Aiouache and Goto (2003) [26]	–	74.0	–	Amberlyst™ 15	< 0.44 mm
Bozga et al.(2008) [17]	–	69.3±5.3	–	Amberlyst™ 35	Commercial
Boonthamtirawuti et al. (2009) [49]	–	103.1	–	Amberlyst™ 16	< 0.55 mm

[a] TAEE formation from 2M1B (R2). [b] TAEE formation from 2M2B (R3).

Table 8. Vaporization, gas and liquid phase adsorption enthalpies of reactants.

Compound	$\Delta_v H^o_j$ [kJ/mol]	$\Delta_{ads} H^o_{j,(g)}$ [kJ/mol]	$\Delta_{ads} H^o_{j,(l)}$ [kJ/mol]
IB	22.2[a]	–60.2[c]	–38
EtOH	42.3[b]	–43.5[c]	–1.2
2M1B	28.5[a]	–71.9[c]	–43.4
2M2B	28.4[a]	–76.9[c]	–48.5

[a]From National Institute of Standards and Technology (NIST) book [52].
[b]Average of 12 experimental values from NIST book. [c]Experimental values determined for A-15 [53].

Table 9. Activation energies for etherification reactions.

Reaction	E'_a [kJ/mol]	E_a (LHHW) [kJ/mol]	E_a (ER) [kJ/mol]
R1	72.8	109.6	71.6

R2	74.9	117.1	73.7
R3	81.2	128.5	80.0

Figure captions

Figure 1. Chemical reactions

Figure 2. Effect of internal and external mass transfer. T=353 K, $R^{o}_{A/O}$=1, $R^{o}_{C4/C5}$=1, and 1g of A-35. Error bars refer to 95% confidence level

Figure 3. Evolution of the reactants conversion with respect to the contact time for different catalyst loads. T=353 K, $R^{o}_{A/O}$=1, $R^{o}_{C4/C5}$=1, 600 rpm, d_p=0.25-0.4 mm. Dashed lines are guides to the eye

Figure 4. Experimental mole evolution obtained under different conditions: (a) T=353.5 K, $R^{o}_{A/O}$=1, $R^{o}_{C4/C5}$=1, 0.29 g A-35; (b) T=342.8 K, $R^{o}_{A/O}$=0.5, $R^{o}_{C4/C5}$=1, 0.41 g A-35; (c) T=352.7 K, $R^{o}_{A/O}$=2, $R^{o}_{C4/C5}$=2, 0.27 g A-35; (d) T=323.2 K, $R^{o}_{A/O}$=1, $R^{o}_{C4/C5}$=1, 1.54 g A-35. Dashed lines are guides to the eye

Figure 5. (a) r_{ETBE} and (b) r_{TAEE} vs. reaction time at different temperatures. $R^{o}_{A/O}$=1, $R^{o}_{C4/C5}$=1. Error bars refer to 95% confidence level for replicated experiments. Dashed lines are guides to the eye

Figure 6. Comparison of experimental and predicted reaction rates using (a) Eq. 16, and (b) Eq. 17

Figure 7. Arrhenius plot of kinetic terms for reactions R1, R2, R3 and R4

Figures

Figure 1

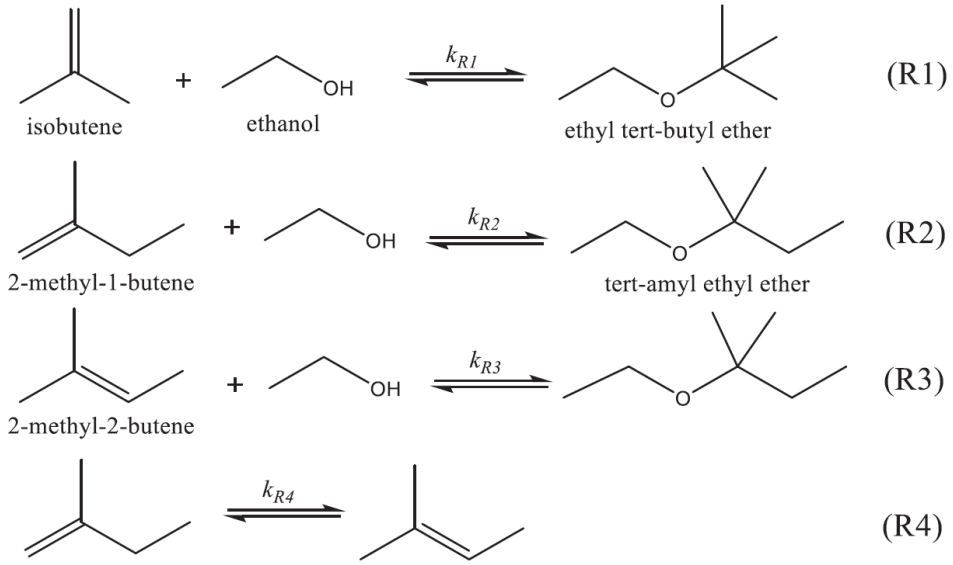

Figure 2

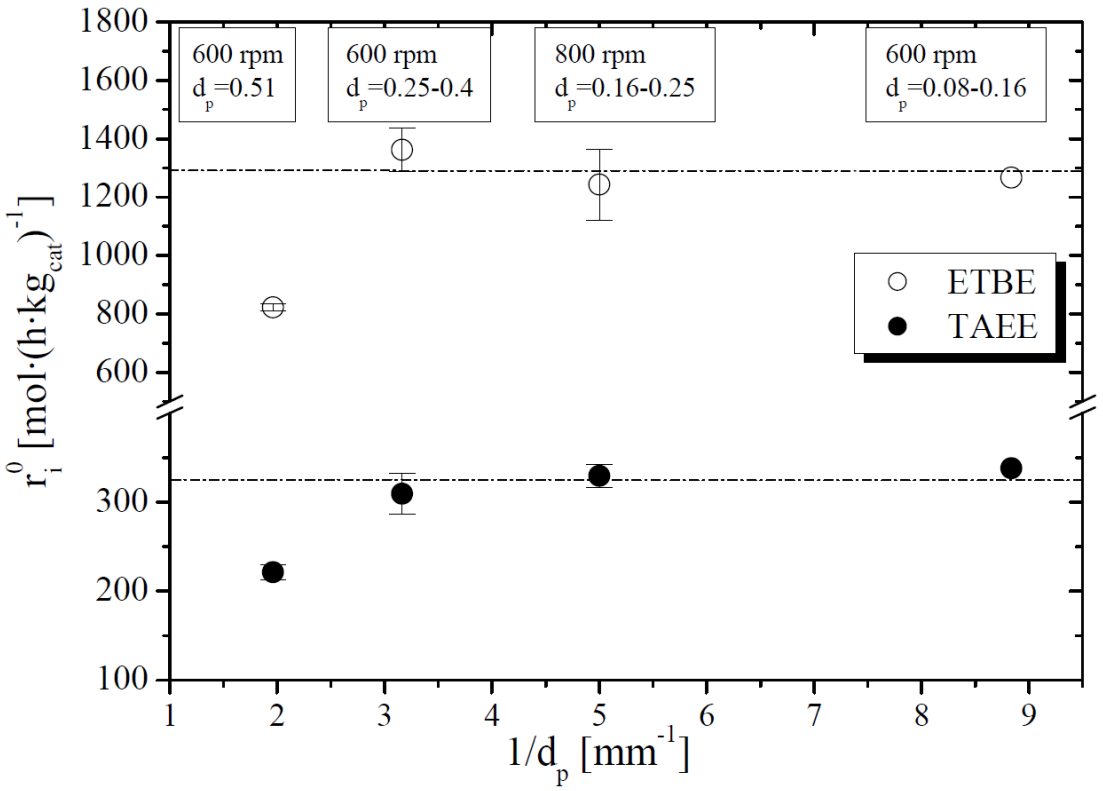

Figure 3

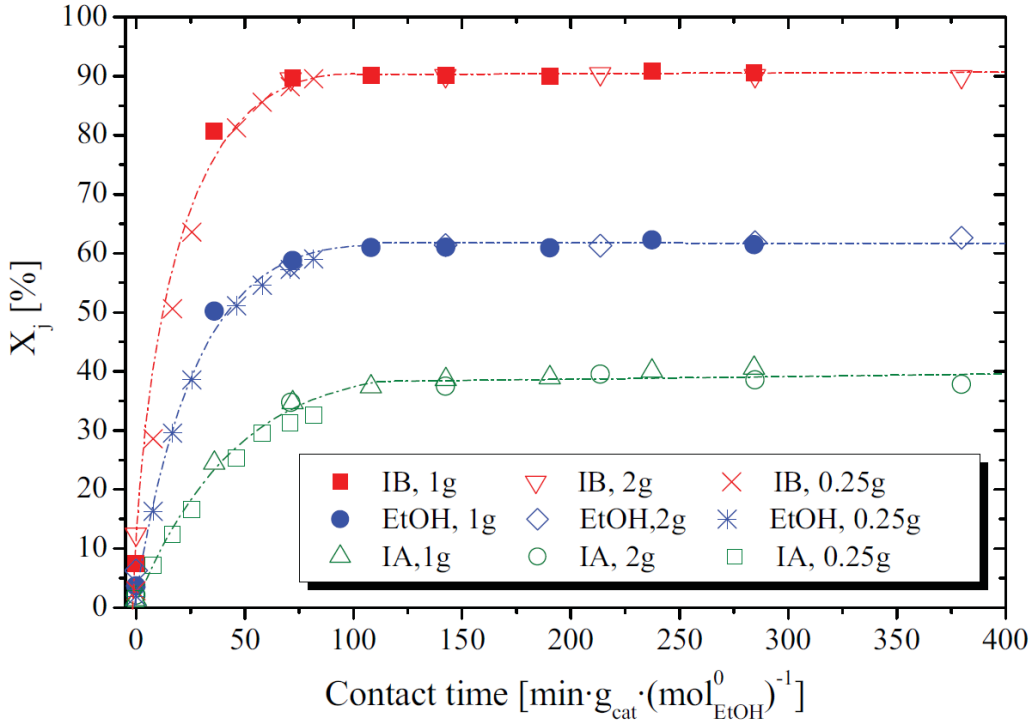

Figure 4

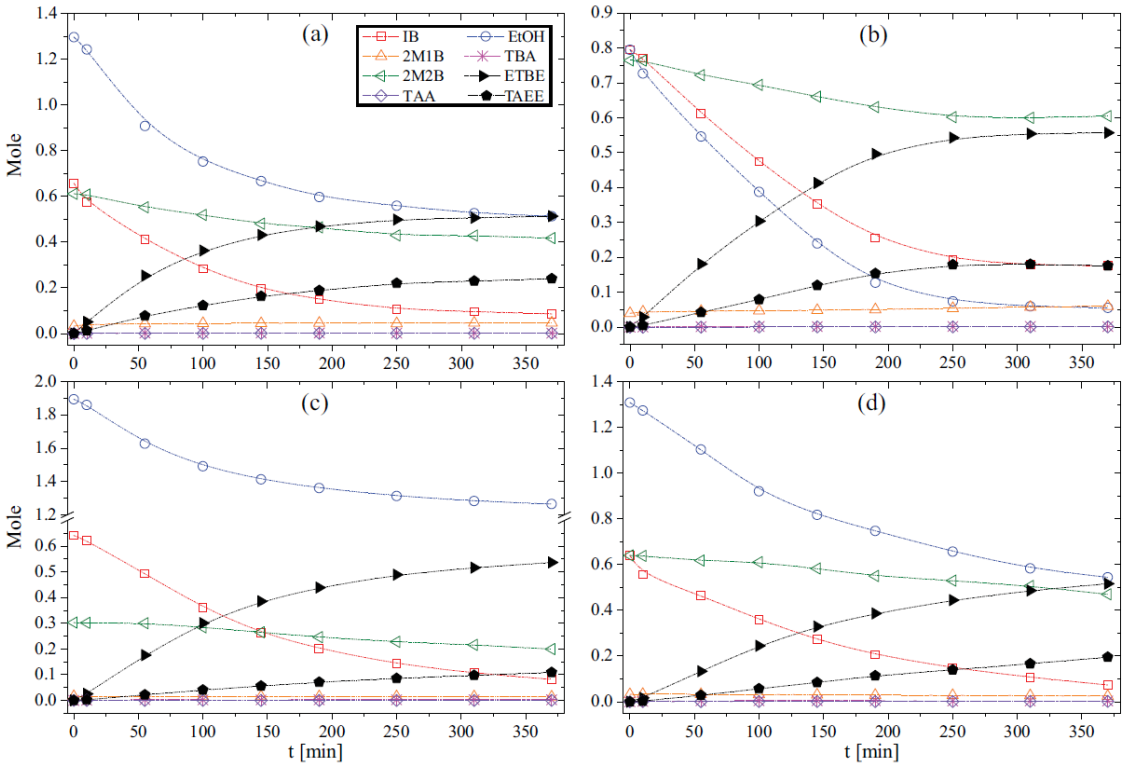

Figure 5

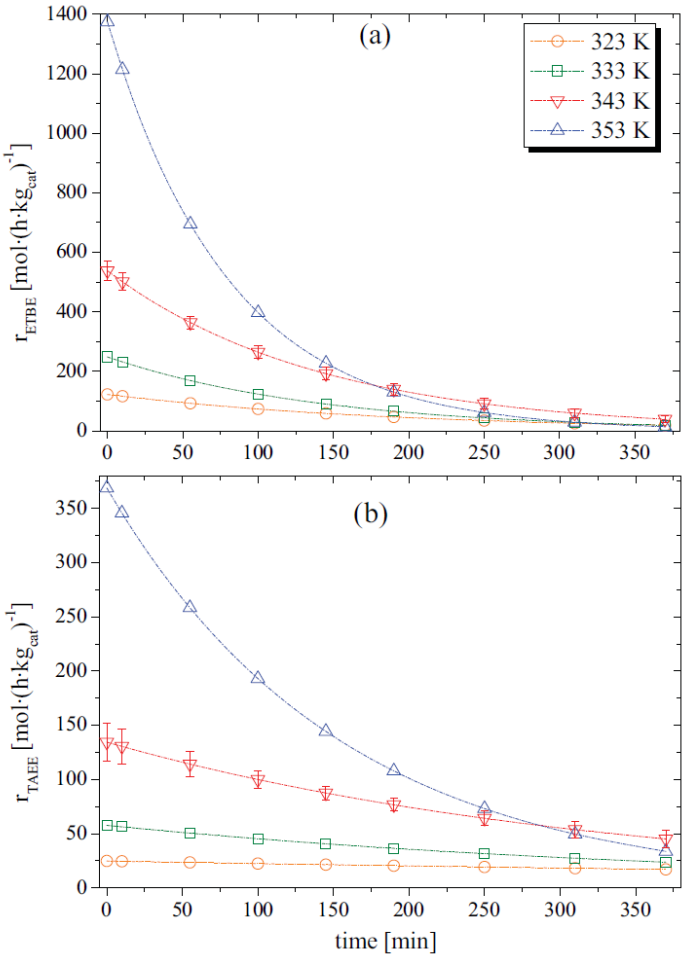

Figure 6

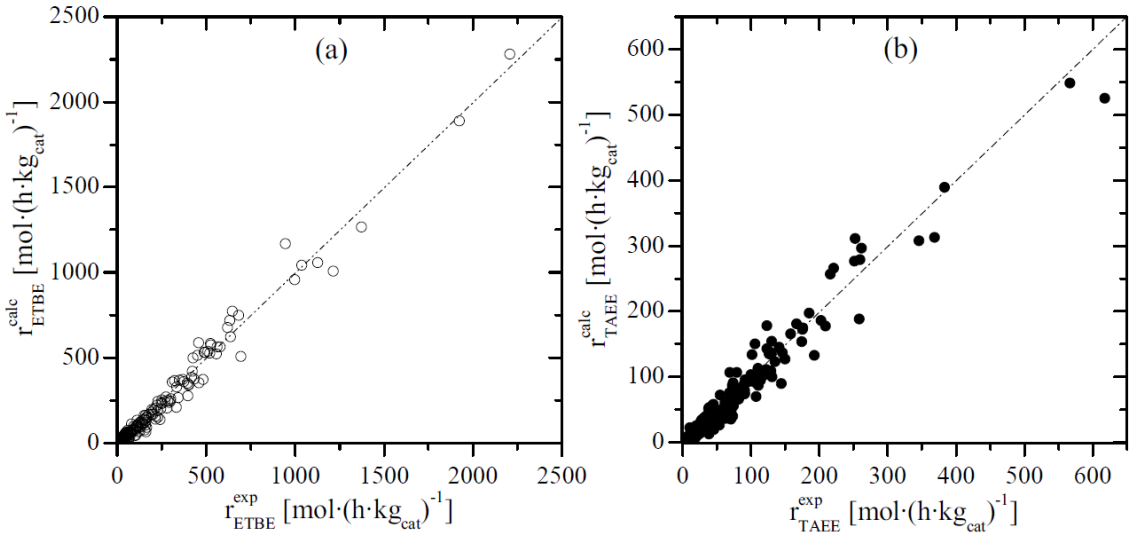

Figure 7

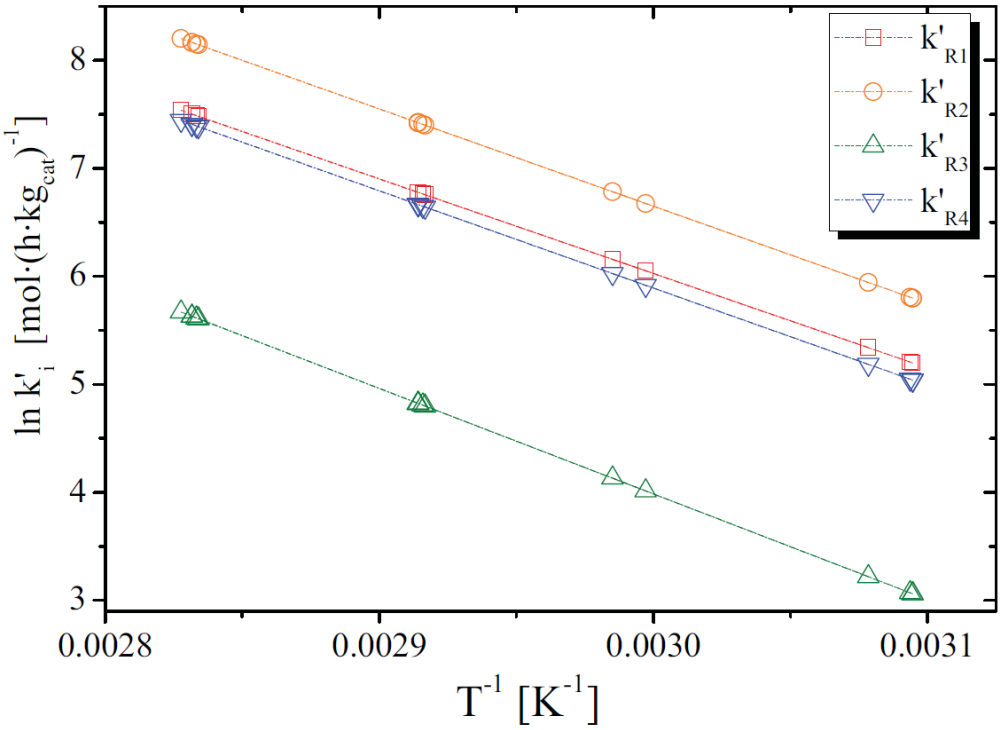
k'R1
k'R2
k'R3
k'R4
ln k'i [mol·(h·kgcat)-1]
T-1 [K-1]
8
7
6
5
4
3
0.0028
0.0029
0.0030
0.0031

Supplementary material

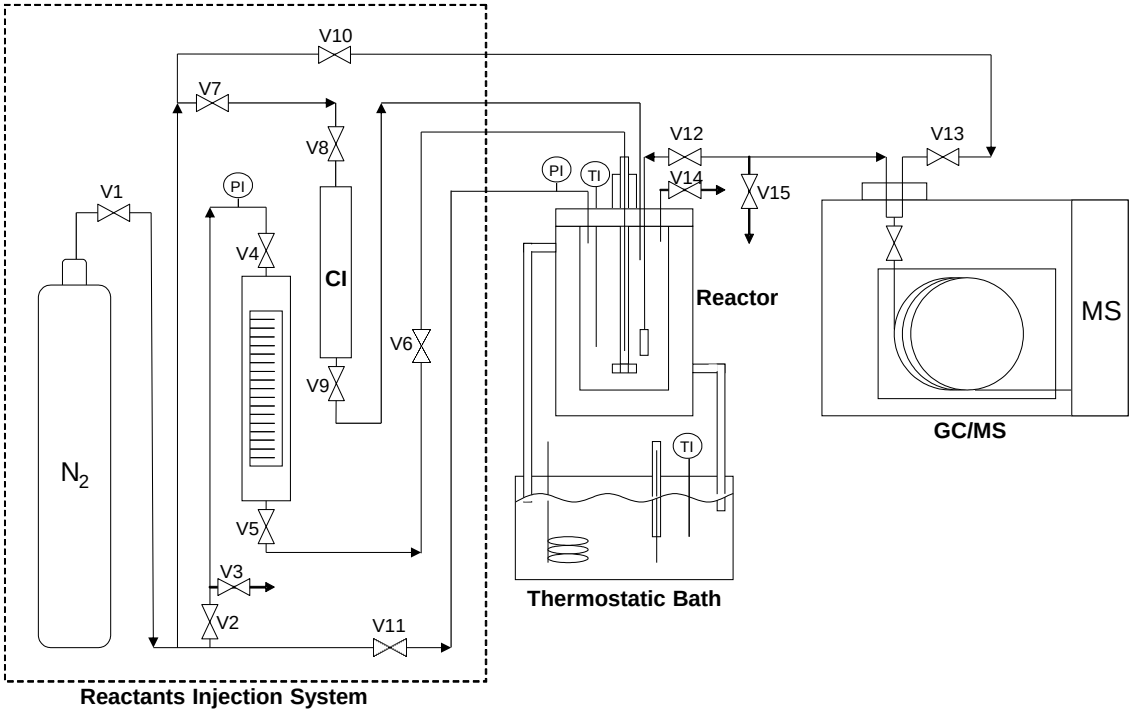

Figure A1. Detailed scheme of the experimental setup. V1-V15: Valves. GC/MS: Gas Chromatograph/Mass Spectrometer. CI: Catalyst Injector. PI: Pressure Indicator (Manometer). TI: Temperature Indicator (Thermocouple).